RSC Advances

PAPER

View Article Online
View Journal | View Issue

Cite this: *RSC Adv.*, 2017, **7**, 31239

Direct synthesis of platinum nanodots in ZIF-8/Fe_3O_4 core–shell hybrid nanoparticles†

Sanghee Lee, Changyong Yim and Sangmin Jeon *

Received 27th April 2017
Accepted 13th June 2017

DOI: 10.1039/c7ra04711h

rsc.li/rsc-advances

A novel method was developed for synthesizing platinum nanodots inside zeolitic imidazolate framework nanostructures without using additional reducing agents. Fe_3O_4 magnetic nanoparticle clusters (MNCs) were synthesized and coated with ZIF-8 (ZIF) shells *via* a hydrothermal reaction. Upon addition of ZIF/MNC hybrid nanoparticles into a platinum precursor (K_2PtCl_4) solution, platinum ions were reduced to metallic platinum nanodots by the 2-methyl imidazolate groups. The resulting platinum nanodots were ~2 nm in diameter and uniformly distributed in the pores of the ZIF layer. The catalytic activity of the platinum nanodots was examined by using Pt/ZIF/MNCs for the reduction of 4-nitrophenol. The resulting high catalytic activity was attributed to the high surface area of the platinum nanodots and the absence of capping layers. Furthermore, the hybrid nanoparticles were recovered using a permanent magnet and were found to maintain their catalytic activity after multiple cycles.

Introduction

Platinum has been widely used as a catalyst in fuel cells, the petroleum industry, and catalytic converters in automobiles owing to its high catalytic activity for various chemical and electrochemical reactions.[1–3] The high price of platinum, however, limits widespread utilization, and transition metal-based catalysts have been explored as alternatives.[4,5] Since no alternative catalyst yet developed can compete with platinum, a method to efficiently and economically utilize precious platinum is required. The best way to simultaneously meet the catalytic activity and economic viability of platinum is to load platinum nanoparticles on high-surface-area-supporting materials such as porous silica.[6–9]

Loading platinum nanoparticles into porous materials can be achieved by incorporating platinum nanoparticles into porous materials or by reducing platinum ions to platinum nanoparticles.[10–12] The direct incorporation of platinum nanoparticles, however, has a drawback wherein uniform distribution of the particles inside porous materials is difficult.[13,14] The reduction of platinum ions inside porous materials has a drawback of the need to use reducing agents, inducing formation of platinum nanoparticles outside the supporting material, and the need to use capping agents to block the active sites of the particles, degrading the catalytic performance.[15] In addition, heat treatment after loading of platinum nanoparticles into porous silica induces aggregation of the nanoparticles, reducing their active surface area.[16,17]

Metal–organic frameworks (MOFs) may be a good alternative to conventional porous silica materials because they do not require thermal treatment owing to their crystalline structure. Among MOFs, a zeolitic imidazolate framework (ZIF) has recently attracted much attention owing to its high surface area, well-ordered pore structures, easy synthesis, and high chemical and thermal stability.[18–22] Numerous studies have been reported on the synthesis of metal nanoparticles inside ZIF, but they used reducing agents for the synthesis or simply encapsulated platinum nanoparticles.[23–25]

In this study, we report a novel route for synthesizing platinum nanodots inside ZIF-8 without the use of reducing agents or capping agents. The reduction of platinum ions to metallic platinum nanodots was induced by 2-methyl imidazolate groups. We synthesized platinum nanodots inside ZIF-8-coated Fe_3O_4 magnetic nanoparticle clusters (ZIF/MNCs), and the resulting platinum nanodots were ~2 nm in diameter and uniformly distributed in the pores of the ZIF layer (Pt/ZIF/MNCs). The catalytic activity of the platinum nanodots was examined using Pt/ZIF/MNCs for the reduction of 4-nitrophenol. The high catalytic activity was attributed to high surface area of the platinum nanodots and the absence of capping layers. Furthermore, Pt/ZIF/MNCs were magnetically recovered after the reaction and were found to maintain their catalytic activity.

Experimental

Chemicals

Iron(III) chloride hexahydrate ($FeCl_3 \cdot 6H_2O$), sodium citrate, urea, polyacrylamide (PAM), zinc nitrate hexahydrate

Department of Chemical Engineering, Pohang University of Science and Technology (POSTECH), Pohang, Gyeongbuk, Republic of Korea. E-mail: jeons@postech.ac.kr

† Electronic supplementary information (ESI) available. See DOI: 10.1039/c7ra04711h

($Zn(NO_3)_2 \cdot 6H_2O$), 2-methylimidazole, imidazolate sodium derivative, potassium tetrachloroplatinate (K_2PtCl_4), and 4-nitrophenol were purchased from Sigma-Aldrich (St. Louis, MO, USA) and used as received without further treatment. Deionized (DI) water (18.3 MΩ cm) was obtained from a reverse osmosis water system (Human Corporation, Korea).

Synthesis of Fe_3O_4 magnetic nanoparticle clusters (MNCs)

MNCs were synthesized using a one-pot hydrothermal method. In brief, 1.6 g of $FeCl_3 \cdot 6H_2O$, 3.48 g of sodium citrate, and 1.06 g of urea were dissolved in 20 mL of water to which 0.37 g of PAM in 20 mL water was added. After stirring the solution for several hours, it was transferred to a Teflon-lined stainless steel autoclave. The hydrothermal synthesis reaction was conducted at 200 °C for 12 h, and the autoclave was allowed to cool naturally to room temperature (RT). The precipitated MNCs were collected using a permanent magnet, washed several times with DI water, and dried overnight under reduced pressure.

Synthesis of ZIF-8 shell on MNC (ZIF/MNC)

0.05 g of MNCs were dissolved in 30 mL of methanol and mixed with 0.15 g of $Zn(NO_3)_2 \cdot 6H_2O$, 0.657 g of 2-methylimidazole, and 10 μL of hydrochloric acid solution. The addition of HCl induces the protonation of 2-methylimidazolate, which leads to the slow formation of ZIF-8 shells on MNCs. The synthesis of ZIF-8 shells on MNCs was conducted under sonication at 60 °C for 10 min and the resulting ZIF/MNC was rinsed several times with ethanol and dried overnight inside a vacuum oven at 50 °C.

Synthesis of Pt nanodots inside the pores of ZIF-8 shells (Pt/ZIF/MNC)

Platinum nanodots were synthesized inside the pores of ZIF-8 shells by adding 2 mg mL^{-1} ZIF/MNC nanoparticles into a 6 mg mL^{-1} K_2PtCl_4 aqueous solution. The reaction was allowed to continue for 48 h at RT under gentle shaking. Then, the synthesized nanoparticles were rinsed several times with DI water and dried under reduced pressure. Scheme 1 illustrates the synthetic procedure of Pt/ZIF/MNC nanoparticles and their application for the reduction of 4-nitrophenol to examine the catalytic activity of platinum nanoparticles.

Catalytic reduction of 4-nitrophenol using Pt/ZIF/MNCs

4-Nitrophenol (1 mM, 100 μL) was added to 1.29 mL of deionized water and mixed with a sodium borohydride solution (100 mM, 600 μL). After 10 μL of Pt/ZIF/MNC nanoparticles (1 mg mL^{-1}) were added to the solution, the UV-Vis absorbance spectrum was measured as a function of reaction time. To examine the reusability of the nanoparticles, they were magnetically collected using a permanent magnet after the reaction and the reduction was repeated five times. The catalytic activity of Pt/ZIF/MNC for each cycle was calculated by measuring the difference in the absorbance at 400 nm before and after 15 min of reaction time.

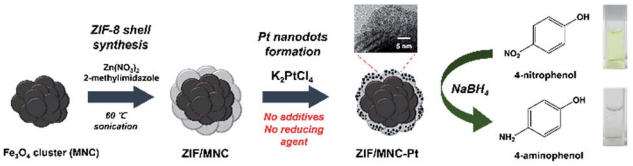

Scheme 1 Schematic of the synthetic procedure for Pt/ZIF/MNC nanoparticles and their application for catalytic reduction of 4-nitrophenol.

Results & discussions

Characterization of Pt/ZIF/MNCs

Fig. 1a and d show scanning electron microscopy (SEM) and transmission electron microscopy (TEM) images of MNCs, respectively. The average size of the MNCs was ~200 nm with a narrow size distribution, and each MNC comprised hundreds of ~15 nm Fe_3O_4 nanoparticles. The magnetic separation efficiency increases with the size of Fe_3O_4 nanoparticles, but Fe_3O_4 loses its paramagnetic properties at sizes >30 nm and assumes ferromagnetic properties, making them difficult to re-disperse in solution after magnetic separation. To avoid this problem, MNCs were used in this study instead of single large Fe_3O_4 particles. The formation of a ZIF-8 shell on MNCs (see Fig. 1b and e for SEM and TEM images of ZIF/MNC, respectively) increased the diameter of the MNCs by 40 nm. In contrast, the ZIF shells were partially dissolved during the reduction of platinum ions (see Fig. 1c and f for SEM and TEM images of Pt/ZIF/MNC, respectively) due to the low pH of the platinum precursor solution (pH = 4.9). The structure of Pt/ZIF/MNCs remained after the subsequent catalytic reduction of 4-nitrophenol. Fig. 1g shows the saturation magnetization curves of MNC, ZIF/MNC, and Pt/ZIF/MNC. The saturation magnetization value of MNC (66.8 emu g^{-1}) decreased to 32.3 emu g^{-1} after the formation of the ZIF-8 shells. The saturation magnetization

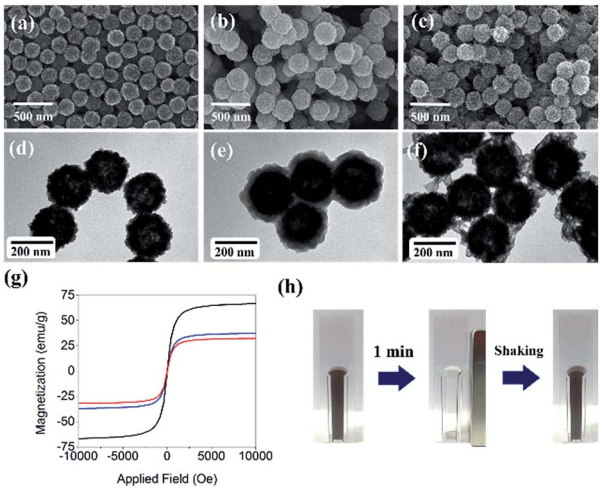

Fig. 1 SEM and TEM images of MNC (a and d), ZIF/MNC (b and e), and Pt/ZIF/MNC (c and f), respectively. (g) Saturation magnetization curves of MNC (black), ZIF/MNC (red), and Pt/ZIF/MNC (blue). (h) Optical images of magnetic separation of Pt/ZIF/MNC nanoparticles using a permanent magnet.

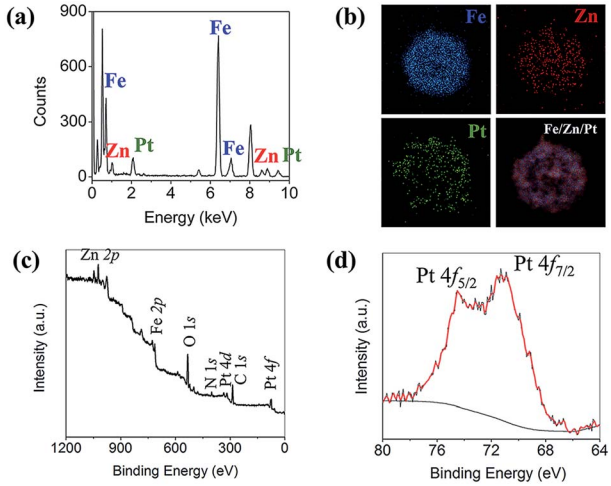

Fig. 2 (a) Energy dispersive X-ray spectrum (EDS) of Pt/ZIF/MNCs. (b) EDS elemental mappings of a single Pt/ZIF/MNC. (c) XPS survey spectrum of Pt/ZIF/MNCs. (d) XPS spectra of Pt 4f level (red).

value of Pt/ZIF/MNC increased to 37.3 emu g^{-1} due to the partial dissolution of the ZIF-8 layer. Although Pt/ZIF/MNCs possess a lower saturation magnetization value than as-synthesized MNCs, ~99% separation was achieved within 1 min using a permanent magnet (Fig. 1h).

Further characterization of Pt/ZIF/MNC was conducted using energy dispersive X-ray spectroscopy (EDS) and X-ray photoelectron spectroscopy (XPS). Fig. 2a shows the chemical composition of Pt/ZIF/MNC examined by EDS. Major peaks in the spectrum correspond to iron, zinc, and platinum, derived from MNC, ZIF-8, and platinum nanodots, respectively. The atomic ratio of Pt : Zn : Fe was determined to be 6.4 : 4.1 : 89.5. Fig. 2b shows EDS elemental mapping images of a single Pt/ZIF/MNC. Iron appeared in the center of the hybrid nanoparticles, whereas zinc and platinum appeared in the shell of the nanoparticles. XPS analysis was conducted to measure the elemental composition of the synthesized hybrid nanoparticles (Fig. 2c). According to the XPS survey spectrum, the chemical compositions of Fe, O, Zn, N, and Pt in ZIF/MNC–Pt nanoparticles were well matched to those obtained from EDS. The XPS spectra in Fig. 2d demonstrates that the binding energy of Pt ($4f_{5/2}$ = 74.5 eV and $4f_{7/2}$ = 71.2 eV) is similar to that of bulk Pt, indicating that the platinum precursor was reduced to metallic Pt.

Characterization of Pt nanodots in ZIF-8 shell

Fig. 3a and b show a TEM image of Pt/ZIF/MNC and its magnified image of the ZIF-8 layer, respectively. The thickness of the ZIF-8 shell is ~15 nm; the shell contains a number of uniformly and densely distributed platinum nanodots. The high-resolution TEM (HR-TEM) image in Fig. 3c and reduced Fast Fourier Transform (FFT) pattern in the inset confirm that the platinum nanodots are highly crystalline. The spacing between parallel lattice fringes (0.24 nm) corresponds to the (111) plane of platinum. Crystalline structures of the nanoparticles were also investigated by powder X-ray diffraction analysis (Fig. S1†); the diffraction peaks of MNCs were well

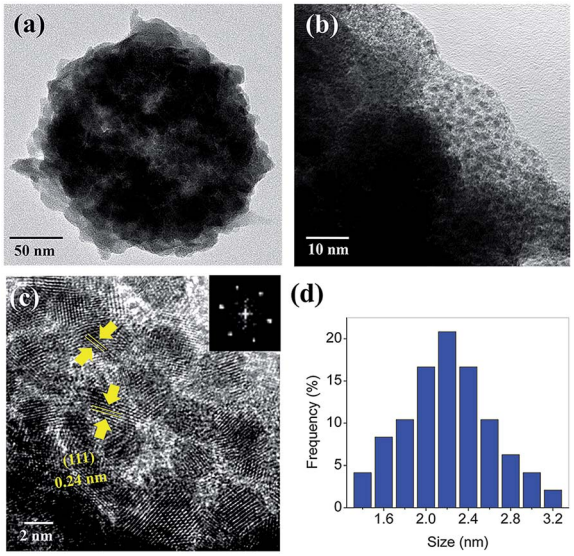

Fig. 3 (a) TEM image of Pt/ZIF/MNC nanoparticle. (b) Magnified TEM image of the ZIF-8 shell in Pt/ZIF/MNC. (c) HR-TEM image of platinum nanodots in ZIF/MNC. The inset shows a reduced FFT pattern of a single Pt nanodot. (d) Size histogram of platinum nanodots encapsulated in the ZIF-8 shell.

matched with those of magnetite phase of Fe_3O_4 according to JCPDS 11-0614. Fig. 3d shows the size histogram of the platinum nanodots. The average size was calculated to be 2.21 ± 0.42 nm.

Fig. 4a–d show HR-TEM images of Pt/ZIF/MNCs as a function of reaction time. The size of the platinum nanodots increased to 1, 2.2, and 2.8 nm after 24, 48, and 72 h of the reaction, respectively. Of note, the reduction of platinum nanoparticles occurred without the addition of any reducing agents or additives. Control experiments were conducted to investigate which functional groups in the ZIF/MNCs are responsible for the reduction. The reduction of K_2PtCl_4 was performed using 2-

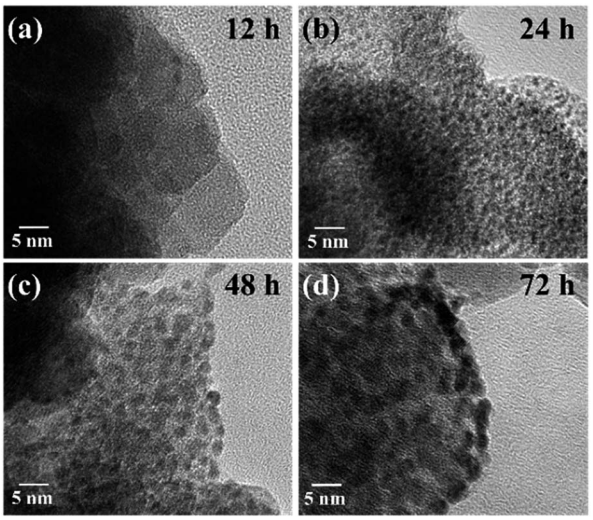

Fig. 4 HR-TEM images of platinum nanodots in a ZIF-8 shell as a function of the reaction time; (a) 12 h, (b) 24 h, (c) 48 h, and (d) 72 h.

methylimidazole or MNC; however, they did not reduce the platinum ions, indicating that simple imidazole and MNC are not responsible for the reduction. In contrast, the reduction of K_2PtCl_4 was observed using ZIF-67 (Co), which comprise cobalt ions coordinated to 2-methyl imidazolate, or ZIF-7 and ZIF-90, which comprise zinc ions coordinated with different types of imidazolate linkers (Fig. S2†). In addition, the reduction was achieved by the addition of sodium imidazolate to K_2PtCl_4 solution (Fig. S2e†). These results indicate that the reduction of platinum ions was induced by imidazolate. As platinum nanoparticles grow with the reaction time, they merged with the adjacent nanoparticles and the number of nanoparticles decreased. The slow reduction suppressed the random aggregation of platinum nanoparticles and resulted in uniform growth of platinum nanoparticles with a narrow size distribution.

Catalytic activity of Pt/ZIF/MNC

To evaluate the catalytic activity of Pt/ZIF/MNC nanoparticles, they were used for the reduction of 4-nitrophenol. Fig. 5a shows optical images of a cuvette containing 4-nitrophenol before and after addition of the hybrid nanoparticles and $NaBH_4$. As the reduction progresses, the solution color changes from yellow to transparent. The UV-Vis absorbance spectrum was measured every 1 min to quantify the degree of the reaction (Fig. 5b). The intensity of the absorption peak at 400 nm decreased to almost zero within 15 min of the reaction, whereas a new peak appeared at ~300 nm owing to the transformation of 4-nitrophenol to 4-aminophenol. The high catalytic activity of the platinum was attributed to the high surface area of the platinum nanodots and facilitated diffusion of reactant molecules through the interconnected pore networks of ZIF. Fig. 5c shows that the logarithms of the normalized intensity of the absorption peak changes are linear with respect to reaction time, indicating that the catalytic reduction of 4-nitrophenol may follow pseudo-first-order kinetics. The apparent rate constant was calculated from the slope to be 5.57×10^{-3} s^{-1}, comparable or higher than previously reported values.[26–28] The Pt/ZIF/MNC nanoparticles were magnetically collected and used for subsequent reactions to examine if the catalytic activity of Pt was maintained. Fig. 5d shows a normalized conversion efficiency of a 4-nitrophenol solution for five consecutive reduction reactions using recycled Pt/ZIF/MNC nanoparticles. The Pt/ZIF/MNC nanoparticles showed >95% conversion efficiency after five cycles of use. The slight decrease in catalytic activity of the recycled nanoparticles is attributed to the loss of particles during magnetic separation.

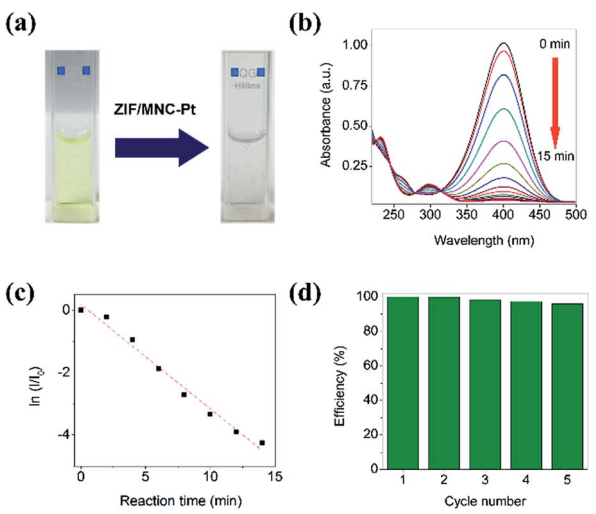

Fig. 5 (a) Optical images of cuvettes containing 4-nitrophenol solution before and after the reduction using Pt/ZIF/MNC nanoparticles for 15 min. (b) UV-Vis absorbance spectrum of a 4-nitrophenol solution as a function of reaction time. Each curve was obtained every 1 min of the reaction. (c) Logarithms of the normalized intensity of the absorption peak as a function of reaction time. (d) Normalized conversion efficiency of 4-nitrophenol solution for five consecutive reduction reactions using recycled Pt/ZIF/MNC nanoparticles.

Conclusions

We developed a novel method for synthesizing platinum nanodots inside ZIF shells of ZIF/MNC hybrid nanoparticles without using reducing agents or additives. 2-Methyl imidazolate was found to reduce platinum precursors to metal nanoparticles. The high catalytic activity of platinum was attributed to high surface area of the platinum nanodots and the absence of capping layers. Further, the facilitated diffusion of reactant molecules through the interconnected pore networks of ZIF might increase the catalytic activity. As this new method does not require any reducing agents or additives for the reduction of platinum ions, it is simpler and more efficient than previously reported methods. Further, fast magnetic separation of nanoparticles is advantageous for recycling the hybrid nanoparticles when used in various practical applications.

Acknowledgements

This work was supported by the Industrial Strategic Technology Development Program (10070241, Fabrication of High Bulk Porous Composite Sorbent with Pulp Support for Removal of Oil and Heavy Metals by Wet-laid Process) funded By the Ministry of Trade, Industry & Energy (MOTIE, Korea).

Notes and references

1 Y. Mu, H. Liang, J. Hu, L. Jiang and L. Wan, *J. Phys. Chem. B*, 2005, **109**, 22212–22216.
2 H. Liu, C. Song, L. Zhang, J. Zhang, H. Wang and D. P. Wilkinson, *J. Power Sources*, 2006, **155**, 95–110.
3 K.-Q. Peng, X. Wang, X.-L. Wu and S.-T. Lee, *Nano Lett.*, 2009, **9**, 3704–3709.
4 C. Parmeggiani and F. Cardona, *Green Chem.*, 2012, **14**, 547–564.
5 G. Wu and P. Zelenay, *Acc. Chem. Res.*, 2013, **46**, 1878–1889.
6 S. H. Joo, S. J. Choi, I. Oh, J. Kwak, Z. Liu, O. Terasaki and R. Ryoo, *Nature*, 2001, **412**, 169–172.
7 S. H. Joo, J. Y. Park, C.-K. Tsung, Y. Yamada, P. Yang and G. A. Somorjai, *Nat. Mater.*, 2009, **8**, 126–131.

8 Y. Li, Y. Li, E. Zhu, T. McLouth, C.-Y. Chiu, X. Huang and Y. Huang, *J. Am. Chem. Soc.*, 2012, **134**, 12326–12329.
9 S. Wu, J. Liu, Z. Tian, Y. Cai, Y. Ye, Q. Yuan and C. Liang, *ACS Appl. Mater. Interfaces*, 2015, **7**, 22935–22940.
10 H. Song, R. M. Rioux, J. D. Hoefelmeyer, R. Komor, K. Niesz, M. Grass, P. Yang and G. A. Somorjai, *J. Am. Chem. Soc.*, 2006, **128**, 3027–3037.
11 N.-I. Kim, J. Y. Cheon, J. H. Kim, J. Seong, J.-Y. Park, S. H. Joo and K. Kwon, *Carbon*, 2014, **72**, 354–364.
12 L. Yang, K. L. Tate, J. B. Jasinski and M. A. Carreon, *ACS Catal.*, 2015, **5**, 6497–6502.
13 C.-K. Tsung, J. N. Kuhn, W. Huang, C. Aliaga, L.-I. Hung, G. A. Somorjai and P. Yang, *J. Am. Chem. Soc.*, 2009, **131**, 5816–5822.
14 X. Guo, L. Li, X. Zhang and J. Chen, *ChemElectroChem*, 2015, **2**, 404–411.
15 J. N. Kuhn, C.-K. Tsung, W. Huang and G. A. Somorjai, *J. Catal.*, 2009, **265**, 209–215.
16 S. Chytil, W. R. Glomm, E. Vollebekk, H. Bergem, J. Walmsley, J. Sjöblom and E. A. Blekkan, *Microporous Mesoporous Mater.*, 2005, **86**, 198–206.
17 Y. Li, B. P. Bastakoti, H. Abe, Z. Liu, A. Minett, Z. A. Alothman and Y. Yamauchi, *RSC Adv.*, 2015, **5**, 97928–97933.
18 G. Lu and J. T. Hupp, *J. Am. Chem. Soc.*, 2010, **132**, 7832–7833.
19 Y. Pan, Y. Liu, G. Zeng, L. Zhao and Z. Lai, *Chem. Commun.*, 2011, **47**, 2071–2073.
20 K. Liang, R. Ricco, C. M. Doherty, M. J. Styles, S. Bell, N. Kirby, S. Mudie, D. Haylock, A. J. Hill and C. J. Doonan, *Nat. Commun.*, 2015, **6**, 7240.
21 C. Yim, M. Lee, W. Kim, S. Lee, G.-H. Kim, K. T. Kim and S. Jeon, *Chem. Commun.*, 2015, **51**, 6168–6171.
22 A. Schejn, T. Mazet, V. Falk, L. Balan, L. Aranda, G. Medjahdi and R. Schneider, *Dalton Trans.*, 2015, **44**, 10136–10140.
23 G. Lu, S. Li, Z. Guo, O. K. Farha, B. G. Hauser, X. Qi, Y. Wang, X. Wang, S. Han and X. Liu, *Nat. Chem.*, 2012, **4**, 310–316.
24 P. Wang, J. Zhao, X. Li, Y. Yang, Q. Yang and C. Li, *Chem. Commun.*, 2013, **49**, 3330–3332.
25 C. J. Stephenson, J. T. Hupp and O. K. Farha, *Inorg. Chem. Front.*, 2015, **2**, 448–452.
26 Q. Wang, Y. Zhang, Y. Zhou, Z. Zhang, Y. Xu, C. Zhang and X. Sheng, *New J. Chem.*, 2015, **39**, 9942–9950.
27 W. Gao, S. Li, M. Pal, Y. Liu, X. Wan, W. Li, S. Wang, C. Wang, G. Zheng and D. Zhao, *RSC Adv.*, 2016, **6**, 61064–61072.
28 X. Liu, D. Chen, L. Chen, R. Jin, S. Xing, H. Xing, Y. Xing and Z. Su, *Chem.–Eur. J.*, 2016, **22**, 9293–9298.